JOURNAL OF CATALYSIS 100, 360–376 (1986)

Comparative Kinetic Studies of $CO-O_2$ and CO–NO Reactions over Single Crystal and Supported Rhodium Catalysts

SE H. OH,* GALEN B. FISHER,* JOYCE E. CARPENTER,*,[1] AND D. WAYNE GOODMAN†

*Physical Chemistry Department, General Motors Research Laboratories, Warren, Michigan 48090-9055; and †Surface Science Division, Sandia National Laboratories, Albuquerque, New Mexico 87185

Received August 19, 1985; revised March 20, 1986

The kinetics of the $CO-O_2$ and CO–NO reactions over single crystal Rh(111) and over alumina-supported Rh catalysts have been compared at realistic reactant pressures. For the $CO-O_2$ reaction, there is excellent agreement between both the specific rates and activation energies measured for the two types of Rh catalysts. The CO–NO reaction, on the other hand, exhibits substantially different activation energies and specific reaction rates between the single crystal and supported catalysts. This indicates that the kinetics of the CO–NO reaction, unlike the $CO-O_2$ reaction kinetics, are sensitive to changes in catalyst surface characteristics. The kinetic data for the $CO-O_2$ and CO–NO reactions over Rh(111) and Rh/Al_2O_3 were analyzed using mathematical models which account for the individual elementary reaction steps established from surface chemistry studies of the interactions of CO, NO, and O_2 with Rh surfaces. The model, when used with the parameter values similar to those reported in the surface chemistry literature, can *quantitatively* fit the CO oxidation rate data over both the single crystal and supported Rh catalysts. The kinetics of the CO–NO reaction over Rh(111) can also be well described by a reaction model using parameter values taken from surface chemistry studies. However, the rate data for the CO–NO reaction over supported Rh can be rationalized by assuming that the dissociation of molecularly adsorbed NO occurs much more slowly on supported Rh than on Rh(111).

I. INTRODUCTION

During the past 2 decades, the application of various modern surface science techniques for fundamental catalytic studies has advanced our understanding of the mechanism of elementary surface reactions on the atomic scale and the relationship of surface characteristics (i.e., structure and composition) to catalytic properties. Most surface-sensitive techniques require an ultrahigh vacuum environment and are best suited for studying well-characterized low surface area materials such as metal single crystals of the size of ~1 cm^2. Many catalytic processes of practical interest, on the other hand, are catalyzed by active metals dispersed on a high surface area oxide support (typically 100–200 m^2/g) under atmospheric conditions. Because of these differences in the nature of the catalyst materials and in the pressure regimes, questions have frequently been raised regarding the applicability of the information obtained on idealized surfaces of single crystals to catalysis occurring on high surface area supported catalysts. Establishing the correlation between single crystal and supported catalyst systems is of considerable practical as well as scientific importance. Good correlations between these two catalyst systems would allow the utilization of the wealth of chemical information obtained from model catalyst studies to gain a detailed understanding of complex "real" catalyst systems. Such understanding can be useful in improving existing catalysts or in the development of new catalysts.

As a step toward bridging the pressure gap mentioned above, several experimental systems have recently been developed (*1*, *2*) which consist of a high-pressure reaction chamber linked to an ultrahigh vacuum

[1] Present address: AC Spark Plug Division, General Motors Corp., Flint, Mich. 48556.

0021-9517/86 $3.00

(UHV) analysis chamber. The unique feature of such an apparatus is the capability of conducting both high-pressure kinetic measurements and UHV surface characterization without removing the sample from the controlled atmosphere. Such experimental systems have been used to measure the kinetics of a number of important reactions, such as the methanation reaction over nickel single crystals (*3, 4*) and polycrystalline rhodium (*5*), cyclopropane hydrogenation over platinum single crystals (*5*), and ethane hydrogenolysis over nickel single crystals (*6*). Comparisons of these model catalyst kinetic data with the reaction rates measured over supported catalysts in the same reactant environment show that the methanation and hydrogenation reactions are structure-insensitive (i.e., no significant variation in reaction rate with changes in catalyst surface morphology), whereas ethane hydrogenolysis is structure-sensitive.

The purpose of this paper is to report the results of a kinetic study of the $CO-O_2$ and CO–NO reactions over a supported Rh/Al_2O_3 catalyst and to compare them with those of a parallel kinetic study (*7*) of the same reactions conducted under similar conditions on a model Rh(111) catalyst. Considerable attention was given to matching the reaction conditions between the two Rh catalyst systems. The comparison of kinetic data under conditions where the only difference is the catalyst (Rh(111) or Rh/Al_2O_3) has allowed us to discuss some important issues regarding the relevance of surface science to catalysis.

In this paper, we will first address the question of "structural sensitivity" by comparing the kinetics of each of the two reactions over the two different types of Rh catalysts under identical operating conditions (i.e., same catalyst temperature and reactant partial pressures). Besides their importance in the catalytic control of automobile exhaust emissions, these two reaction systems provide interesting examples of differing structure sensitivity. As will be shown in this paper, the kinetics of the $CO-O_2$ reaction over Rh(111) and Rh/Al_2O_3 show striking similarities whereas the CO–NO reaction exhibits drastically different kinetic behavior (i.e., different activation energy, specific rate, and order of the reaction) over the two Rh catalysts. The second objective of this study is to analyze the kinetic data using a mathematical model which accounts for the individual elementary reaction steps involved in the $CO-O_2$ and CO–NO reactions. The underlying assumption in our model development was that the basic reaction mechanisms established from surface chemistry studies of Rh single crystals under UHV conditions remain valid for supported Rh catalysts operating under realistic high-pressure conditions.

II. EXPERIMENTAL

The apparatus used for kinetic measurements over Rh(111) single crystals has previously been described in detail (*2, 3, 7*), so only the salient features of the system will be summarized here. It consists of a high-pressure (up to ~2 atm) reaction chamber linked to a UHV surface analysis chamber. The catalyst sample is mounted on a retraction bellows and can be translated *in situ* from the reactor to the surface analysis chamber. The single crystals were spot-welded to two short high-purity tungsten leads and heated resistively. High-purity gases, carefully cleaned, were used for kinetic measurements. Gas chromatography (flame ionization detection) provided a convenient and sensitive technique for the analysis of the reaction products, and Auger Electron Spectroscopy (AES) was used to characterize the catalyst surface before and after reaction rate measurements.

The supported Rh catalyst used in the experiments was prepared by impregnating Grace low-density θ-alumina beads (3.3 mm diameter, 110 m^2/g BET surface area) to incipient wetness with an aqueous solution of $RhCl_3$. After impregnation the catalyst was dried in air overnight at room temperature and calcined in air at 500°C for 4 h. The nominal Rh loading was 0.01 wt% and the

Rh was deposited in a shallow band (~30 μm) at the periphery of the catalyst beads. The Rh dispersion of the catalyst was determined to be 12% from CO chemisorption measurements based on 2 : 1 stoichiometry between adsorbed CO molecules and surface Rh atoms. This chemisorption stoichiometry is based on the infrared spectroscopic observation of the dominance of $Rh(CO)_2$ species (*8, 9*) for low-loaded Rh/Al_2O_3 catalysts such as ours. It is worth mentioning that the CO chemisorption measurements were carried out following all the kinetic experiments reported here and thus the Rh dispersion number quoted above represents the property of the stabilized catalyst that had been used over an extended period of time (1 year or so). We assume that the chemisorption stoichiometry did not change significantly with the use, because the highest temperature the catalyst was exposed to during the rate measurements was 450°C and thus sintering of the Rh catalyst is expected to be minimal.

The steady-state reaction rates over the Rh/Al_2O_3 catalyst were measured using an internal-recycle mixed flow reactor (*10*) operating at atmospheric total pressure. The reactor is made of stainless steel, and gas-phase mixing within the reactor is provided by a magnetically driven impeller placed under the stationary catalyst basket. All the data reported here were obtained at an impeller speed of 1500 rpm; this impeller speed was found to be high enough to establish gradientless conditions in the gas phase under our experimental conditions (typically a total feedstream flow rate of 5 liters/min (STP) through 4.4 g of Rh/Al_2O_3). The partial pressures of the individual reactants were matched to those used in the model catalyst kinetic experiments by blending appropriate amounts of the gases in a N_2 background.

The steady-state composition of the inlet and outlet gases of the mixed flow reactor was measured using continuous gas analyzers (nondispersive IR for CO and CO_2, polarographic detection for O_2, chemiluminescence detection for NO). Reaction rates were then calculated directly from the difference between the measured inlet and outlet concentrations using the well-known material balance equation for well-mixed reactors.

III. SURFACE CHEMISTRY REACTION MODEL

In this section we develop the reaction models for the $CO–O_2$ and CO–NO reactions on Rh. After a discussion of the reaction mechanisms and the rate expressions of the individual elementary reaction steps, we present the steady-state conservation equations for the surface species. The overall reaction rates can then be computed from the surface concentration values satisfying the conservation equations.

A. $CO–O_2$ Reaction

It is generally established [see Ref. (*11*) for a recent review] that the catalytic oxidation of CO on noble metals occurs primarily through a Langmuir–Hinshelwood reaction (rather than an Eley-Rideal mechanism) between largely immobile adsorbed oxygen atoms and adsorbed CO molecules which are mobile on the catalyst surface. The interaction of oxygen with Rh is complex; molecular adsorption (*12–14*), dissociative chemisorption (*12–15*), and oxide formation (*16–19*) are all possible on a given surface depending on the temperature and pressure regimes under consideration. Molecular adsorption has been observed on Rh(111) for adsorption at 100 K and this molecular state has been suggested as a mobile precursor to dissociative chemisorption of oxygen (*12, 13*). In the temperature range where CO oxidation has an appreciable rate, however, no molecularly adsorbed O_2 has been observed (*12–14*) and thus this form of oxygen will not be included explicitly in the reaction steps. Surface oxides can form on Rh(111) during high-temperature (~1000 K) treatments in high-pressure oxygen (*16*) and the oxidation of supported Rh has been shown to occur much more

readily (>400 K in a net-oxidizing environment) (*18–19*).

Furthermore, this oxide formation has been reported to alter the adsorptive/catalytic properties of Rh (*16–18, 20*). Thus the presence of Rh oxide species on the catalyst surface under reaction conditions can complicate the interpretation of the kinetics of CO oxidation over Rh catalysts. In view of this complication, a large excess of oxygen over CO was avoided during the rate measurements, especially with the Rh/Al_2O_3 catalyst, in order to ensure that chemisorbed atomic oxygen (rather than Rh oxides) is the dominant surface oxygen species and is primarily responsible for the catalytic oxidation of CO.

Based on the discussion given above, the mechanism of CO oxidation on Rh can be represented by the reaction sequence

$$CO \rightleftarrows CO_a \quad (1)$$

$$O_2 \rightarrow 2O_a \quad (2)$$

$$CO_a + O_a \rightarrow CO_2 \quad (3)$$

The subscript "a" refers to species adsorbed on the Rh surface, while the variables without a subscript denote gas-phase species. Notice that the O_2 desorption step is neglected in our model, so that surface oxygen can be removed only through the Langmuir–Hinshelwood step shown in Eq. (3). This simplification is reasonable in view of the negligibly slow O_2 desorption rate at temperatures of interest in this study (<600 K) (*12–15*).

Preliminary analysis of our CO oxidation rate data indicates that they were all obtained in the CO inhibition regime where the catalyst surface is predominantly covered with CO. This condition is expected to prevail even when O_2 is in moderate excess over CO, because CO is adsorbed much more strongly on the Rh surface than oxygen. In developing rate expressions for each of the above individual elementary steps, then, we will focus on the limiting case of interest here, namely a CO-covered surface with a small concentration of adsorbed oxygen atoms.

The rates of adsorption of CO ($r_{CO,ads}$) or oxygen ($r_{O_2,ads}$) on the catalyst surface can be readily obtained from the kinetic theory of gases (*21, 22*).

$$r_{CO,ads} = \sqrt{\frac{R_g T}{2\pi M_{CO}}}\,\sigma S_{CO} C_{CO} \theta_v \equiv k_{CO,ads} C_{CO} \theta_v \quad (4)$$

$$r_{O_2,ads} = \sqrt{\frac{R_g T}{2\pi M_{O_2}}}\,\sigma S_O C_{O_2} \theta_v \equiv k_{O_2,ads} C_{O_2} \theta_v \quad (5)$$

where the fraction of vacant sites, θ_v, on the CO-covered surface can be approximated by

$$\theta_v = 1 - \theta_{CO}. \quad (6)$$

The coefficient σ is the area occupied by 1 mol of surface metal atoms (3.75×10^8 cm^2/mol for Rh(111)). In Eq. (5) the O_2 adsorption rate is taken to be proportional to θ_v (rather than the expected θ_v^2 dependence) in view of the recent observation of Yates *et al.* (*23*) that the θ_v dependence better describes the rate of O_2 adsorption on Rh(111). This observation can be explained by an O_2 adsorption mechanism where the rate-controlling step involves the initial interaction of an O_2 molecule with a single Rh site, with rapid subsequent dissociation of the adsorbed O_2 molecules. Our choice of first-order O_2 adsorption kinetics is further supported by our kinetic data; as will be discussed below, second-order O_2 adsorption kinetics cannot match the CO oxidation rate data even with arbitrary adjustments of parameter values. Linear adsorption kinetics of oxygen have also been observed on Pd(111) (*24*) and Pt(111) (*25*).

It should be noted that the surface coverage dependence of the adsorption rates described by Eqs. (4)–(6) is not strictly valid for systems involving precursor adsorption (*26, 27*); however, this should be a reasonable approximation to the adsorption behavior at the high CO-coverage limit.

The rate of CO desorption, $r_{CO,des}$, can be expressed as

$$r_{CO,des} = A \exp[-(E - \alpha_{CO}\theta_{CO})/R_gT]\theta_{CO} \equiv k_{CO,des}\theta_{CO} \quad (7)$$

assuming that the activation energy for CO desorption decreases linearly with CO coverage. This linear coverage dependence of the desorption activation energy is often used in the analysis of thermal desorption data (*27–29*) and can be related physically to the repulsive interaction between adsorbed CO molecules (*30*). Although both the preexponential factor and activation energy for desorption are generally dependent on the surface coverage (*31, 32*), we will assume a constant preexponential factor in the present analysis for the sake of simplicity. Equation (7) is a crude first approximation to reality since it implicitly assumes the presence of only one kind of adsorbed CO species on the surface. Nevertheless, it provides a reasonable description of CO desorption behavior at the high CO-coverage limit of interest here.

The rate expression for the Langmuir–Hinshelwood reaction (or CO_2 formation) step, r_{CO_2}, is taken to be of the form

$$r_{CO_2} = A \exp[-E/R_gT]\theta_{CO}\theta_O. \quad (8)$$

The steady-state conservation equations for the surface species CO_a and O_a are

$$r_{CO,ads} - r_{CO,des} - r_{CO_2} = 0 \quad (9)$$

$$2r_{O_{2,ads}} - r_{CO_2} = 0 \quad (10)$$

Once Eqs. (9) and (10) are solved for θ_{CO} and θ_O (using, for example, Newton's iteration method) for specified values of T, C_{CO}, and C_{O_2}, the rate of CO oxidation can readily be calculated from r_{CO_2} given in Eq. (8). This rate represents the number of CO_2 molecules produced per surface metal atom per second (i.e., turnover number). For the limiting case of $\theta_{CO} \approx 1$, the above steady-state conservation equations can easily be manipulated to give the following approximate expression for the rate of CO oxidation:

$$\bar{R}_{CO-O_2} \approx \frac{2k_{O_{2,ads}}}{k_{CO,ads}} \cdot k_{CO,des}(T) \cdot \frac{P_{O_2}}{P_{CO}} \quad (11)$$

where $k_{CO,ads}$, $k_{O_{2,ads}}$, and $k_{CO,des}(T)$ are the rate constants defined in Eqs. (4), (5), and (7), respectively. Note that the relatively strong temperature dependence of $k_{CO,des}$ is explicitly shown in Eq. (11).

B. CO–NO Reaction

On single-crystal and polycrystalline Rh surfaces, NO adsorbs molecularly with a high sticking probability (*13, 33, 34*). Infrared studies of NO adsorption on silica- and alumina-supported Rh (*35–37*) provide further evidence that NO has a stable molecular adsorption state. Temperature-programmed desorption (TPD) studies with both supported and unsupported Rh (*13, 33, 34, 38*) have shown that at elevated temperatures adsorbed NO undergoes extensive dissociation to form N_a and O_a atoms. This NO dissociation process—a key step in the reduction of NO by CO—has a relatively large activation barrier and proceeds via a mechanism which requires a vacant nearest-neighbor site (*13, 33, 38*). TPD studies (*13*) have also identified two different pathways for N_2 formation: the recombination of two adsorbed N atoms (labeled as β-N_2 state) and the reaction of adsorbed N with adsorbed NO (δ-N_2 state). As in the case of the CO–O_2 reaction, the formation of the other reaction product, CO_2, is taken to occur via a Langmuir–Hinshelwood reaction between adsorbed CO and adsorbed atomic oxygen.

The above discussion on the interactions of NO and CO with Rh surfaces suggests that the mechanism of the CO–NO reaction over Rh can be represented by the following set of elementary processes.

$$CO \rightleftarrows CO_a \quad (12)$$

$$NO \rightleftarrows NO_a \quad (13)$$

$$NO_a \rightarrow N_a + O_a \quad (14)$$

$$NO_a + N_a \rightarrow N_2 + O_a \quad (\delta - N_2) \quad (15)$$

$$2N_a \rightarrow N_2 \qquad (\beta - N_2) \qquad (16)$$

$$CO_a + O_a \rightarrow CO_2 \qquad (17)$$

Notice that the above reaction mechanism does not include steps involving the formation and decomposition of isocyanate species (NCO); a recent infrared study by Hecker and Bell (*39*) shows that this species is not directly involved in the catalytic reduction of NO by CO over Rh. Although it is generally assumed that Eq. (15) proceeds via an "N_2O-like" intermediate (*13*), the formation of N_2O itself has not been incorporated into the reaction mechanism proposed above because we observed no N_2O formation over the Rh(111) catalyst during the CO–NO reaction (*7*). Material balance considerations also show that no N_2O was produced during the CO–NO reaction over the supported Rh catalyst.

The rate expression for CO adsorption given in Eq. (4) remains valid for the CO–NO reaction system. However, CO desorption characteristics during the CO–NO reaction are significantly altered by the presence of adsorbed N atoms on the catalyst surface. Root *et al.* (*40*) have observed strong repulsive interactions between CO_a and N_a on the surface during the temperature-programmed reaction (TPR) study of the CO–NO reaction on Rh(111) single crystal surfaces. This CO_a–N_a repulsion was found to decrease the CO desorption activation energy by as much as 30% compared to that on the N_a-free surface (*40*). A similar repulsive interaction was also observed on polycrystalline Rh wire by Campbell and White (*33*). We assume that the activation energy for CO desorption decreases linearly with both CO_a and N_a coverages on the surface. Thus,

$$r_{CO,des} = A \exp[-(E - \alpha_{CO}\theta_{CO} - \alpha_N\theta_N)/R_gT]\theta_{CO}. \qquad (18)$$

The rates of adsorption and desorption of NO ($r_{NO,ads}$ and $r_{NO,des}$) can be expressed as

$$r_{NO,ads} = \sqrt{\frac{R_gT}{2\pi M_{NO}}}\,\sigma C_{NO} S_{NO}\theta_v \qquad (19)$$

$$r_{NO,des} = A \exp[-E/R_gT]\theta_{NO}. \qquad (20)$$

As in the case of the CO–O_2 reaction, surface oxygen is rapidly removed via the CO_2 formation step (Eq. (17)) during the CO–NO reaction, resulting in a very small concentration of adsorbed oxygen atoms on the surface. Hence, the fraction of vacant sites can be approximated by

$$\theta_v = 1 - \theta_{CO} - \theta_{NO} - \theta_N. \qquad (21)$$

In Eq. (20) a constant (i.e., coverage-independent) activation energy for NO desorption is assumed, because NO desorbs in a single narrow peak with its position being independent of coverage (*13*), even in the presence of CO (*40*). Also, the rate of NO dissociation ($r_{NO,diss}$) can be written as

$$r_{NO,diss} = A \exp[-E/R_gT]\theta_{NO}\theta_v \qquad (22)$$

assuming that the dissociation of adsorbed NO molecules requires a vacant nearest-neighbor site (*13, 33, 38*).

The rate expressions for the two pathways for N_2 formation (Eqs. (15) and (16)) are taken to be of the form

$$r_{N_2,\delta} = A \exp[-E/R_gT]\theta_{NO}\theta_N \qquad (23)$$

$$r_{N_2,\beta} = A \exp[-(E - \alpha_N\theta_N)/R_gT]\theta_N^2. \qquad (24)$$

The activation energy for the formation of the δ-N_2 state is assumed to be constant because its desorption peak temperature changed little with initial NO exposures on both the clean and oxygen-covered surfaces during a recent TPD study with Rh(111) (*13*). The coefficient α_N introduced in Eq. (24) accounts for a possible decrease in the activation energy for the N_a recombination step due to repulsive interactions between adsorbed N atoms.

The rate expression for the surface reaction between CO_a and O_a, r_{CO_2}, is taken to be the same as that given in Eq. (8).

The steady-state conservation equations for the surface species CO_a, NO_a, N_a, and O_a are listed below.

$$r_{CO,ads} - r_{CO,des} - r_{CO_2} = 0 \qquad (25)$$

$$r_{NO,ads} - r_{NO,des} - r_{NO,diss} - r_{N_2,\delta} = 0 \qquad (26)$$

$$r_{NO,diss} - r_{N_2,\delta} - 2r_{N_2,\beta} = 0 \quad (27)$$

$$r_{NO,diss} + r_{N_2,\delta} - r_{CO_2} = 0. \quad (28)$$

The rate of the CO–NO reaction (CO + NO $\rightarrow$ CO_2 + $\frac{1}{2}N_2$) can be calculated from r_{CO_2} given in Eq. (8) using the values of θ_{CO} and θ_O satisfying the above conservation equations. The calculated rate represents the turnover number of the reaction (i.e., the number of CO_2 molecules produced per surface Rh atom per second). It will be useful in interpreting the kinetic data to recognize the relationship

$$\tilde{R}_{CO-NO} = r_{CO_2} = 2r_{N_2,\delta} + 2r_{N_2,\beta}. \quad (29)$$

It should be noted that the underlying assumption in our model development described above is random competitive adsorption of reactants on the catalyst surface. Although the formation of adsorbate islands on the surfaces of bulk metals has been shown to be an important factor in determining the reaction kinetics under some conditions [e.g., Ref. (*11*)], we feel that it is unnecessary to include this complication here. For the CO–O_2 reaction, the oxygen coverage is so low that the presence of islands is a moot issue. For the NO–CO reaction, there is good evidence (*40, 41*) that NO and CO form a well-mixed adlayer, ruling out island formation. Furthermore, significant adsorbate islanding may be even less probable on the very small metal crystallites in supported Rh catalysts.

IV. RESULTS AND DISCUSSION

A. *CO–O_2 Reaction over Rh(111) and Rh/Al_2O_3*

Figure 1 compares the CO oxidation rates measured over the single crystal Rh(111) (solid line) and supported Rh/Al_2O_3 (dashed line) catalysts at $P_{CO} = P_{O_2} = 0.01$ atm. The turnover number for the Rh/Al_2O_3 catalyst was obtained by normalizing the measured reaction rates to the total number of Rh *surface* atoms determined from CO chemisorption measurements. Notice that the turnover numbers for Rh(111) traverse four orders of magnitude over a temperature range of 450–600 K. Kinetic measurements over such a wide temperature range with the supported Rh catalyst were not possible due to heat and mass transfer limitations encountered at high temperatures and to analyzer sensitivity limitations encountered at low temperatures, and thus a direct comparison of the kinetic data between the two types of Rh catalysts must necessarily be limited to a relatively small temperature range (475–515 K). Nevertheless, it is clear from Fig. 1 that there is excellent agreement between the two catalyst systems in both the specific reaction rates and apparent activation energies (29 kcal/mol for Rh(111) vs 30 kcal/mol for Rh/Al_2O_3). This indicates that the kinetics of CO oxidation on Rh are not sensitive to changes in catalyst surface characteristics. Similar structure insensitivity (no significant metal particle size effects on activity) was observed for CO oxidation over supported Pt catalysts (*42, 43*), and over supported and bulk Pd catalysts (*44*).

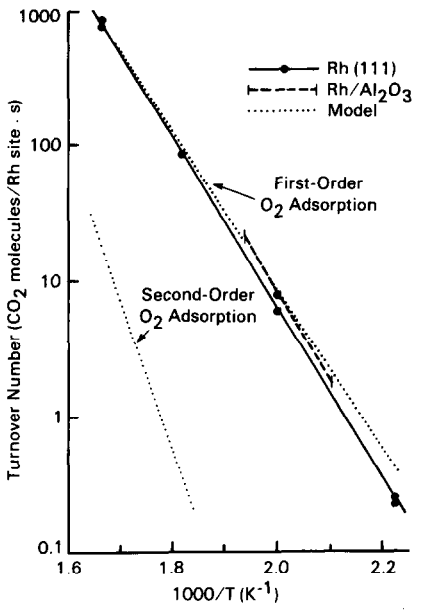

FIG. 1. Comparison of the specific rates of the CO–O_2 reaction measured over Rh(111) and Rh/Al_2O_3 at $P_{CO} = P_{O_2} = 0.01$ atm. Model predictions were obtained using two different oxygen adsorption kinetics.

Also shown in Fig. 1 are the comparisons

of the measured and predicted turnover numbers. The model predictions were obtained using two surface chemistry reaction models; these two models differ only in the surface coverage dependence assumed for the rate of oxygen adsorption. It can be seen that the model prediction based on first-order O_2 adsorption ($r_{O_2,ads} = k_{O_2,ads} C_{O_2}\theta_v$) is in very good agreement with the rate data for both Rh(111) and Rh/Al_2O_3, whereas the model assuming second-order O_2 adsorption kinetics ($r_{O_2,ads} = k_{O_2,ads} C_{O_2}\theta_v^2$) underpredicts the turnover numbers and also overpredicts the apparent activation energy by a wide margin. (This discrepancy in the apparent activation energies makes it impossible to match all the rate data even with arbitrary adjustments of the preexponential factors and sticking coefficients.) These comparisons lend further support to the observation of Yates *et al.* (*23*) that the rate of O_2 adsorption on Rh(111) is proportional to the fraction of vacant sites θ_v rather than to θ_v^2 (which is commonly expected for the direct dissociative chemisorption of a diatomic molecule). In subsequent figures, we will only present the simulation results obtained based on the first-order kinetics of O_2 adsorption.

Table 1 lists the parameter values used in the model calculations and the corresponding values reported in the surface science literature for bulk, unsupported Rh (single crystal Rh(111) or polycrystalline Rh). With the exception of the preexponential factor for the CO_2 formation step (A_{CO_2}), the parameter values used in our model are very similar to the literature values. The value of A_{CO_2} was increased from that reported by Campbell *et al.* (*45*) for the following three reasons. First, their value is several orders of magnitude lower than the typical preexponential factors (10^9–10^{12} s^{-1}) expected for second-order surface reactions (*48*). Another justification for this increase in A_{CO_2} value is based on the results of a recent TPR study of coadsorbed CO and oxygen on Rh(111) (*40*). It was observed in that TPR study that CO_2 is produced in a peak at

TABLE 1

Parameter Values Used in Model Calculations for CO–O_2 Reaction

	This work	Literature value	
CO adsorption			
S_{CO}	0.5	0.5 (*45, 46*)	
CO desorption			
A (s^{-1})	1.6×10^{14}	$1 \times 10^{13.6\pm0.3}$	(*32*)
E (kcal/mol)	31.6	31.6 ± 1	(*32*)
α_{CO} (kcal/mol)	4.5[a]	—	
O_2 adsorption			
S_O (500 K)	0.01	0.01 (*15*)[b]	
CO_2 formation			
A (s^{-1})	1×10^{12}	3×10^5	(*45*)
E (kcal/mol)	14.3	14.3	(*45*)

[a] Estimated from the thermal desorption spectra of CO from Rh(111) (*40*).

[b] Extrapolated from S_O (100 K) = 0.16 (*15*) assuming that S_O decreases with temperature with a reasonable activation energy of ~1 kcal/mol. This value is also consistent with measurements of S_O on a CO-covered surface of Rh(100) for $T \geq 230$ K (*47*).

~425 K (with leading edges beginning at ~350 K) whereas CO desorbs at ~510 K. This indicates that the rate of the surface reaction between CO_a and O_a is much faster than the CO desorption rate. Finally, in view of the relatively high oxygen coverages considered in the experiments of Campbell *et al.* (*45*), it is reasonable to speculate that the small magnitude of their preexponential factor might be related to the presence of oxygen islands on the surface with CO_2 formation proceeding only along the island perimeters. Under our reaction conditions, however, the formation of oxygen islands (and the attendant decrease in the surface reaction rate) is unlikely because the catalyst surface is predominantly covered with CO_a (i.e., very small θ_O). For our calculations, then, the value of A_{CO_2} was arbitrarily set to 10^{12} s^{-1}; determination of the exact value of A_{CO_2} is not crucial for our modeling purposes because model predictions are insensitive to changes in the preexponential value in the regime of our interest ($A_{CO_2} > 10^9$ s^{-1}; see Fig. 2). Model predictions are likewise in-

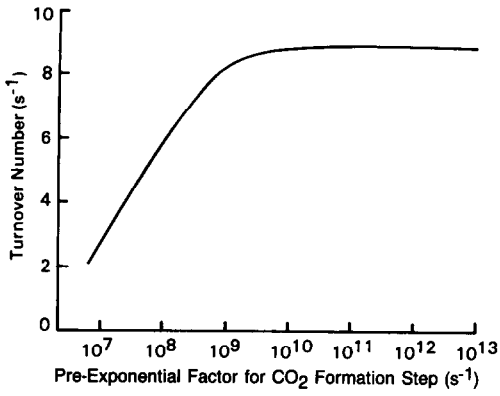

FIG. 2. Effect of the preexponential factor for the CO_2 formation step on the predicted turnover number for the CO–O_2 reaction. $P_{CO} = P_{O_2} = 0.01$ atm, 500 K.

sensitive to variations in the activation energy. This insensitivity of the overall reaction rate to the value of the surface reaction rate constant is consistent with the approximate rate expression for the CO oxidation given in Eq. (11).

Under the conditions of Fig. 1, where the surface is predominantly covered with CO_a ($\theta_{CO} \approx 1$ and very small θ_O), the reaction rate is limited by the adsorption rate of oxygen. As the temperature is increased, the reaction rate increases because more vacant sites become available for oxygen adsorption as a result of the higher CO desorption rate. This explains why the CO oxidation rate in Fig. 1 increases with temperature with an apparent activation energy (29–30 kcal/mol) similar to that for CO desorption. This observation is also in agreement with the temperature dependence of the CO oxidation rate predicted by Eq. (11).

Figure 3 shows how the rate of CO oxidation over the single crystal and supported Rh catalysts depends on the partial pressure of CO. The partial pressure of oxygen (0.01 atm) and catalyst temperature (500 K) were held constant. Here again, the comparison shows extraordinary similarities in kinetic data measured over the two Rh catalyst systems. As expected, the reaction rate is observed to decrease linearly with increasing CO partial pressure (see Eq. (11)). This is a direct consequence of the inhibition of oxygen adsorption caused by a high concentration of CO_a on the surface. Note that both the turnover numbers and the negative first-order dependence of the rate on CO partial pressure are correctly predicted by the model.

We also measured the rate of CO oxidation as a function of oxygen partial pressure at the same catalyst temperature as before (500 K) and at a fixed CO partial pressure of 0.01 atm (see Fig. 4). For $P_{O_2} < 0.1$ atm, the measured rates over both the Rh(111) and Rh/Al_2O_3 catalysts exhibit a first-order dependence on the partial pressure of O_2, as expected from Eq. (11). Again good agreement was obtained between the model predictions and the experimental data. The deviation of the reaction rate from a first-order oxygen dependence at high oxygen partial pressures is not surprising because as the oxygen partial pressure increases, the reaction conditions tend to shift away from the limiting case of the CO-covered

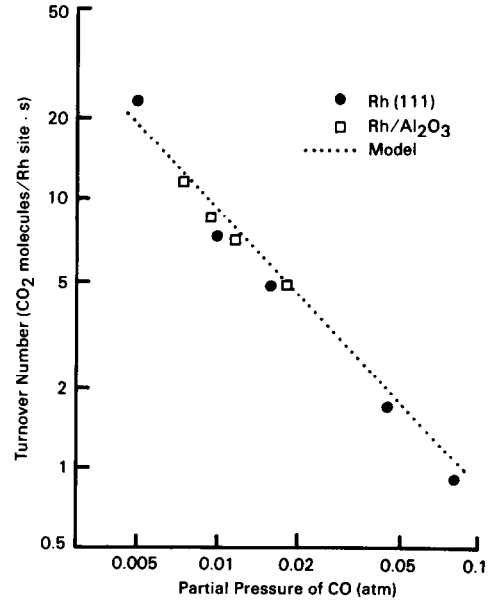

FIG. 3. Measured and predicted rates of the CO–O_2 reaction over Rh(111) and Rh/Al_2O_3 as a function of the partial pressure of CO. The partial pressure of O_2 (0.01 atm) and temperature (500 K) were held constant.

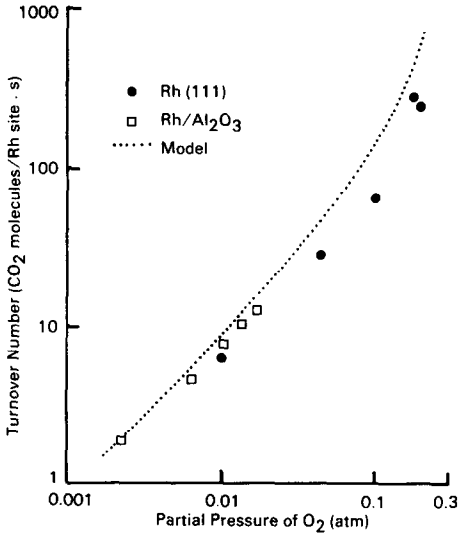

FIG. 4. Measured and predicted rates of the CO–O_2 reaction over Rh(111) and Rh/Al_2O_3 as a function of the partial pressure of O_2. The partial pressure of CO (0.01 atm) and temperature (500 K) were held constant.

surface as a result of the attendant increase in the surface concentration of oxygen.

Equation (11) also suggests that the rate of CO oxidation may depend only on the ratio of the reactant partial pressures (P_{O_2}/P_{CO}) and not on their individual values. This was confirmed by separate experiments with the Rh/Al_2O_3 catalyst where the individual values of P_{CO} and P_{O_2} were varied while holding their ratio constant. The results of such experiments for the case of $P_{O_2}/P_{CO} = 1$ are shown in Fig. 5. The reaction rates measured at the three different sets of reactant partial pressures are virtually the same over the entire temperature range considered (488–510 K), demonstrating that the kinetics of CO oxidation indeed depend only on the ratio P_{O_2}/P_{CO}.

We note that Auger spectroscopic analysis of the Rh single crystal following the CO–O_2 reaction (7) detected no surface oxides for all reaction conditions considered here ($P_{O_2}/P_{CO} < 20$). This rules out the formation of stable Rh oxides or the accumulation of high concentrations of adsorbed oxygen atoms on the Rh(111) surface during the CO–O_2 reaction.

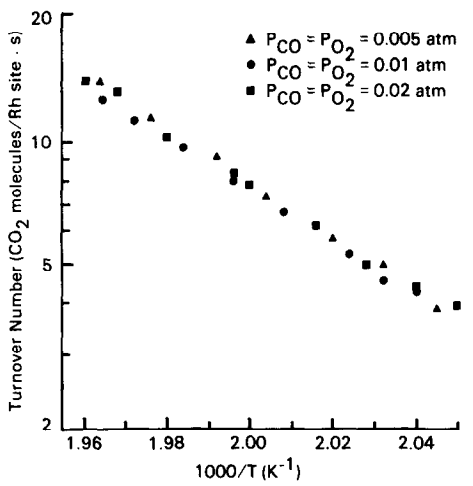

FIG. 5. Rate of the CO–O_2 reaction measured over Rh/Al_2O_3 at a P_{O_2}/P_{CO} ratio of 1.

B. CO–NO Reaction over Rh(111)

Figure 6 compares the rates of the CO–NO reaction measured over the single crystal Rh(111) (closed circles) and supported Rh/Al_2O_3 (dashed line) catalysts at P_{CO} =

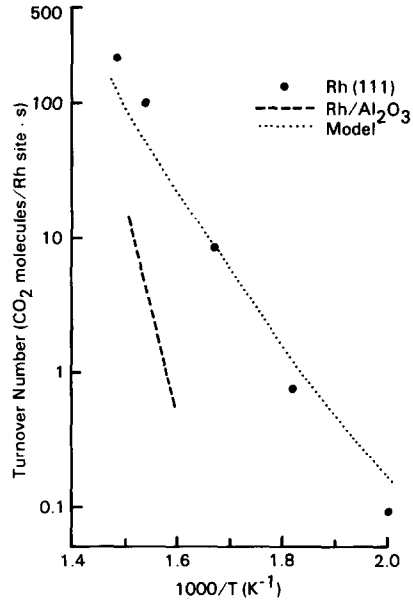

FIG. 6. Comparison of the specific rates of the CO–NO reaction measured over Rh(111) and Rh/Al_2O_3 at $P_{CO} = P_{NO} = 0.01$ atm. The prediction of the surface chemistry model follows closely the rate data for Rh(111).

P_{NO} = 0.01 atm. It is evident in Fig. 6 that there is a dramatic difference between the two types of Rh catalysts in both the apparent activation energies and specific reaction rates. This indicates that the kinetics of the CO–NO reaction, unlike the CO–O_2 reaction kinetics, are sensitive to changes in catalyst surface characteristics. In view of the structure sensitivity observed for the CO–NO reaction, it seems convenient to discuss the single crystal and supported Rh catalysts separately. This section will focus on the kinetic behavior of Rh(111).

Also presented in Fig. 6 (dotted line) are the turnover numbers predicted from the surface chemistry reaction model described in the previous section. The model does a reasonably good job of fitting the rate data for Rh(111), when used with the parameter values determined from experiments with bulk, unsupported Rh (see Table 2). The parameter values for the CO adsorption/desorption and CO_2 formation steps are taken to be the same as those used for the CO–O_2 reaction. Notice, however, that a decrease in the CO desorption activation energy due to N_a–CO_a repulsive interactions is also accounted for in the model for the CO–NO reaction. We increased the value of the preexponential factor for NO desorption from that reported for Rh single crystals because the kinetic behavior observed in the regime of high NO partial pressures (positive-order dependence on P_{NO} as will be shown later) suggests that NO may be adsorbed less strongly on our catalyst sample than indicated by the literature value. Note that the preexponential factor we used for NO desorption is physically reasonable; it is in the order of magnitude expected for the desorption of an adsorbed molecule (*48*).

The model predicts that under the reaction conditions of Fig. 6, the surface of Rh(111) is populated by a high concentration of adsorbed nitrogen atoms and a small but significant amount of molecularly adsorbed NO: θ_N = 0.964, θ_{NO} = 0.035 at 500 K, and θ_N = 0.990, θ_{NO} = 0.003 at 675 K. This prediction of high surface concentrations of N_a is not surprising in view of the rapid NO dissociation on Rh(111) and is consistent with the Auger spectra taken following the reaction, which indicate the presence of significant amounts of nitrogen on the surface (*7*). The surface coverages of CO_a and O_a are predicted to be negligibly small. The low surface concentration of CO can be rationalized based on the increased CO desorption rate resulting from the strong N_a–CO_a repulsive interactions on the Rh(111) surface at high θ_N.

The high surface coverages of N_a predicted above suggest that N_2 desorption is the rate-limiting step for the CO–NO reaction over the single crystal Rh(111) catalyst. As discussed in the previous section, the CO–NO reaction has two competing paths for N_2 formation (i.e., δ-N_2 and β-N_2 steps; see Eqs. (15) and (16)). In this case, then, the reaction kinetics would be domi-

TABLE 2

Parameter Values Used in Model Calculations for CO–NO Reaction

	This work	Literature value	
CO adsorption			
S_{CO}	0.5	0.5 (*45, 46*)	
CO desorption			
A (s^{-1})	1.6×10^{14}	$1 \times 10^{13.6\pm0.3}$	(*32*)
E (kcal/mol)	31.6	31.6 ± 1	(*32*)
α_{CO} (kcal/mol)	4.5	—	
α_N (kcal/mol)	10	10 (*40*)	
CO_2 formation			
A (s^{-1})	1×10^{12}	3×10^{5}	(*45*)
E (kcal/mol)	14.3	14.3	(*45*)
NO adsorption			
S_{NO}	0.5	~1 (*33*)	
NO desorption			
A (s^{-1})	5×10^{13}	2×10^{12}	(*13*)
E (kcal/mol)	26	26	(*13*)
NO dissociation			
A (s^{-1})	6×10^{13}	6×10^{13}	(*41*)
E (kcal/mol)	19	19	(*41*)
δ-N_2 formation			
A (s^{-1})	2×10^{9}	2×10^{9}	(*13*)
E (kcal/mol)	21	21	(*13*)
β-N_2 formation			
A (s^{-1})	3×10^{10}	3×10^{10}	(*13*)
E (kcal/mol)	31	31	(*13*)
α_N (kcal/mol)	4 (estimated)	—	

nated by the path that has a faster rate. A TPD study by Root *et al.* (*34*) suggests that at low temperatures (<~550 K) the CO–NO reaction kinetics is dominated by the δ-N_2 path ($NO_a + N_a \rightarrow N_2 + O_a$; 21 kcal/mol), with little contribution from the β-N_2 path ($N_a + N_a \rightarrow N_2$; 31 kcal/mol). At higher temperatures, on the other hand, the β-N_2 path (due to its higher activation energy and much lower surface coverage of NO_a) would proceed at a faster rate and thus become a controlling pathway for the kinetics of the CO–NO reaction. Generally, such a shift in the controlling step to an alternate, parallel reaction path is accompanied by a rise in activation energy with increasing temperature (*49*). Our mechanistic hypothesis is supported by the results of model calculations in Fig. 6 (dotted curve), which predict a change in the apparent activation energy from ~23 kcal/mol for $T <$ 550 K to ~33 kcal/mol for $T >$ 550 K. However, experimental verification of this mechanism based on the rate data of Fig. 6 is difficult because of the limited number of data points at low temperatures (<550 K). A similar change in activation energy with temperature has been observed by Hecker and Bell (*37*) for the CO–NO reaction over silica-supported Rh.

Figure 7 shows the effect of CO partial pressure on the specific rate of the CO–NO reaction over Rh(111) at 500 K. The partial pressure of NO was held constant at 0.01 atm. The experimental data and model predictions agree well, and they both show that the reaction rate varies only slightly with the partial pressure of CO. This is in sharp contrast to the case of the $CO-O_2$ reaction, where the reaction rate is strongly inhibited by CO. The absence of CO inhibition effects during the CO–NO reaction is not surprising in view of the low surface coverage of CO_a predicted for the Rh(111) surface.

It is important to emphasize that the strong CO_a–N_a repulsive interactions discussed above play a key role in determining the CO–NO reaction kinetics over Rh(111).

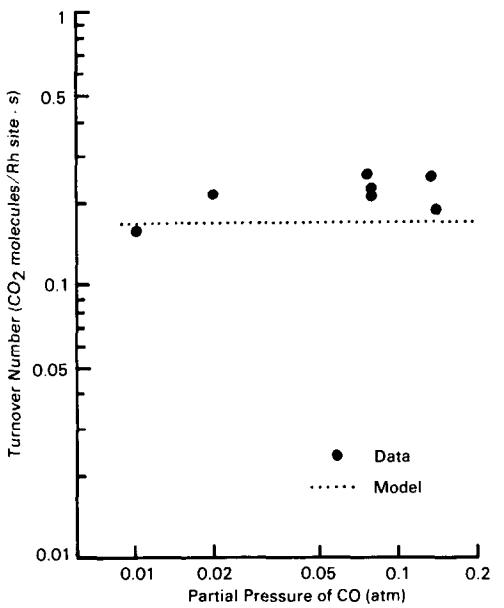

FIG. 7. Measured and predicted rates of the CO–NO reaction over Rh(111) as a function of the partial pressure of CO. The partial pressure of NO (0.01 atm) and temperature (500 K) were held constant.

To illustrate this point, it is instructive to discuss the predictions of the reaction model which neglects the effects of the experimentally observed CO_a–N_a repulsion on CO desorption characteristics (i.e., the model with $\alpha_N = 0$ in Eq. (18); see Fig. 8). As can be seen from comparison of the prediction for $\alpha_N = 0$ with the rate data, such a model is inadequate in describing the kinetic behavior of the CO–NO reaction over Rh(111); the model underpredicts the turnover numbers and fails to predict the observed weak dependence of the rate on the partial pressure of CO. The computed reaction rates for other values of α_N are also included in Fig. 8 to show the sensitivity of the reaction system. Notice that the model predictions become insensitive to variations in α_N values for α_N greater than 10 kcal/mol. The model predictions in Figs. 6 and 7 and in subsequent figures were based on $\alpha_N = 10$ kcal/mol, which closely corresponds to the 30% reduction in the CO desorption activation energy found by Root *et al.* (*40*) for the N_a-covered Rh(111) surface.

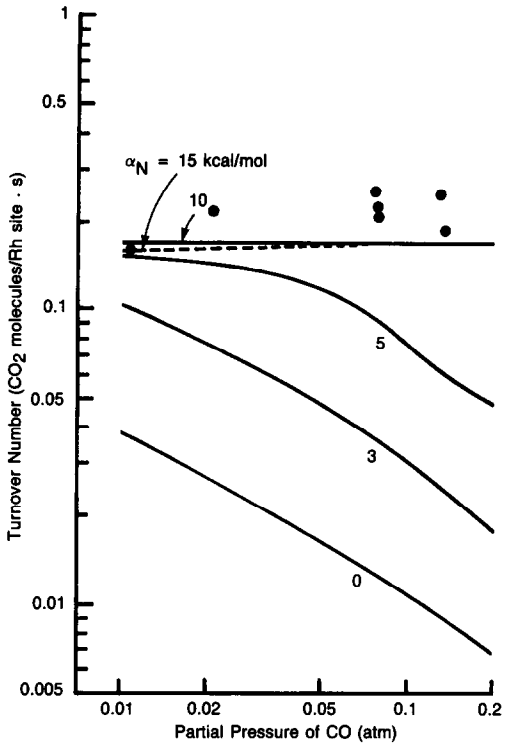

FIG. 8. Predicted rates of the CO–NO reaction over Rh(111) for different values of α_N. The rate data from Fig. 7 (closed circles) are also shown here for comparison. P_{NO} = 0.01 atm, 500 K.

We also conducted kinetic experiments using Rh(111) aimed at investigating the effect of NO partial pressure variation on the CO–NO reaction kinetics. Figure 9 shows the results of such experiments at P_{CO} = 0.01 atm and 500 K, together with the model predictions for Rh(111). Here again the model provides quantitative predictions of the CO–NO reaction rates, including a positive-order dependence on P_{NO}, over the wide range of NO partial pressures considered.

As discussed earlier, the controlling factor for the kinetics of the CO–NO reaction over Rh(111) under the conditions of Fig. 9 (500 K) is most likely to be the rate of δ-N_2 formation, which is proportional to the product of θ_{NO} and θ_N. The observation of a positive-order dependence of the rate on P_{NO} in Fig. 9, then, implies that the surface coverage of NO_a remains moderate (θ_{NO} < 0.5) throughout the NO partial pressure range considered. Indeed, the model predicts that θ_{NO} increases from 0.035 to 0.23 as P_{NO} increases from 0.01 to 0.2 atm. This prediction of relatively low θ_{NO} over the wide range of P_{NO} is reasonable because the majority of NO adsorbed on the Rh(111) surface would not remain in the molecular form but dissociate into N_a and O_a as a result of the fast NO dissociation rate over the Rh single crystal catalyst.

C. CO–NO Reaction over Rh/Al_2O_3

As shown in the Arrhenius plots of Fig. 6, the turnover number and apparent activation energy of the CO–NO reaction over Rh(111) were observed to be drastically different from those over Rh/Al_2O_3. This structure sensitivity of the CO–NO reaction kinetics is further demonstrated by the comparison of the reaction order in P_{NO} over the two types of Rh catalysts. The reaction order in P_{NO} over the Rh/Al_2O_3 catalysts was examined at two different temperatures with a fixed CO partial pressure of

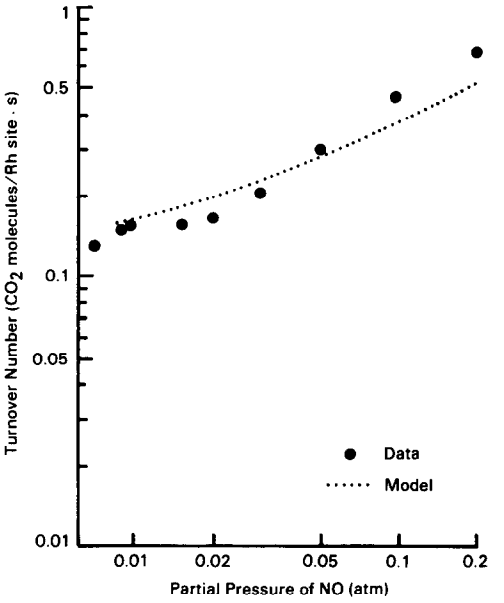

FIG. 9. Measured and predicted rates of the CO–NO reaction over Rh(111) as a function of the partial pressure of NO. The partial pressure of CO (0.01 atm) and temperature (500 K) were held constant.

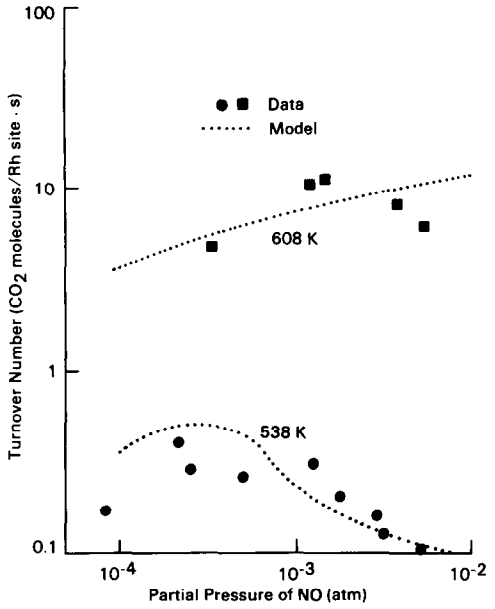

FIG. 10. Measured and predicted rates of the CO–NO reaction over Rh/Al_2O_3 as a function of the partial pressure of NO. The partial pressure of CO (0.01 atm) and temperature were held constant.

0.01 atm. As shown in Fig. 10, the rate of the CO–NO reaction over Rh/Al_2O_3 at 538 K is inhibited by NO at $P_{NO} > \sim 3 \times 10^{-4}$ atm (or ~300 ppm at 1 atm total pressure). This is in sharp contrast to the rate data over Rh(111) presented in Fig. 9, which exhibit a positive-order dependence on P_{NO} up to $P_{NO} = 0.15$ atm under similar reaction conditions. (Rate measurements over Rh/Al_2O_3 at 500 K were not possible because the rates were too low.) In addition, a comparison made in Fig. 10 of the rate data over Rh/Al_2O_3 at 538 and 608 K shows that as the temperature is increased, the critical NO partial pressure at which a transition in the reaction order occurs is shifted to a higher value.

In simulating the supported Rh rate data of Fig. 10, we used the reaction model describing the same reaction steps as presented in the previous section. This amounts to assuming that the mechanism of CO–NO reaction established from surface chemistry studies for unsupported Rh remains valid for supported Rh catalyst systems. All the model parameter values were taken to be the same as those listed in Table 2, with the exception of the rate constant for NO dissociation. This decrease in the NO dissociation rate constant from the Rh(111) value listed in Table 2 is reasonable because the recent infrared and TPD studies of Bell and co-workers (*37, 38*) suggest that for the CO–NO reaction over supported Rh catalysts, the dissociation of NO_a is one of the slowest steps in the reaction sequence. This argument of a low NO dissociation rate is also supported by the theoretical calculations of Miyazaki and Yasumori (*50*). The model predictions shown in Fig. 10 were obtained using a preexponential factor for NO dissociation (3×10^{10} s^{-1}) 2000 times lower than that for Rh(111), while the activation energy for NO dissociation was assumed to remain unchanged. A possible explanation for this adjustment might be that only a small fraction of the total sites on the surface of low-loaded (i.e., highly dispersed) supported Rh catalysts have the capability to dissociate NO because of the requirement of vacant nearest-neighbor sites for the dissociation step (*51*). It can be seen in Fig. 10 that the model predictions compare favorably with the rate data for the two temperatures considered. In particular, the model correctly predicts the strong NO inhibition of the reaction rate observed over the Rh/Al_2O_3 catalyst at 538 K.

Additional comparisons are made in Fig. 11 between measured and predicted rates of the CO–NO reaction over Rh/Al_2O_3 for two different combinations of the partial pressures of CO and NO. In one of the two cases considered, the partial pressure of NO was chosen to be one-tenth that of CO (5×10^{-4} atm NO vs 5×10^{-3} atm CO) in order to approximate the large excess of CO over NO encountered in automobile exhaust. The model calculations were carried out with the same reduced value of the preexponential factor for NO dissociation (3×10^{10} s^{-1}) as was used in Fig. 10. Here again, the model does a good job in predicting the

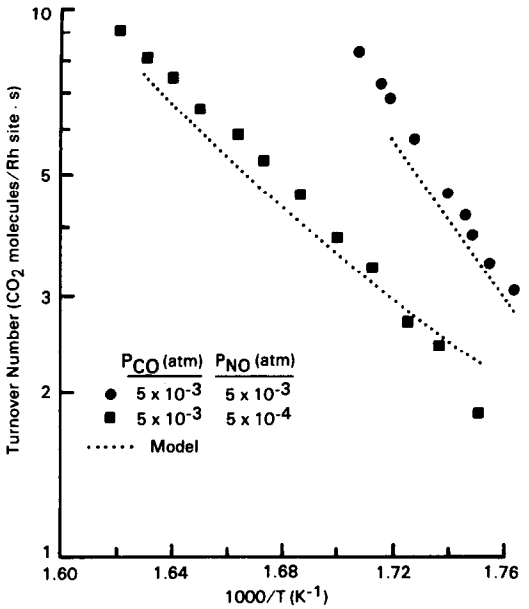

FIG. 11. Arrhenius plots of the measured and predicted rates of the CO–NO reaction over Rh/Al_2O_3 at two different combinations of CO and NO partial pressures.

specific rates and the apparent activation energies for the two cases.

It should be noted that in fitting the supported Rh rate data of Figs. 10 and 11, the Rh surface area that is active for the CO–NO reaction was assumed to be only one-half that for the $CO–O_2$ reaction. This adjustment is qualitatively consistent with the results of an EXAFS study by van't Blik *et al.* (*52*). They found that the Rh in low-loaded Rh/Al_2O_3 catalysts exists as small metal crystallites in the absence of CO on the surface (as in the CO–NO reaction), whereas high surface concentrations of CO (as in the $CO–O_2$ reaction) cause a significant disruption of the Rh crystallites, ultimately leading to isolated Rh atoms (and thereby increasing the active metal surface area).

It is interesting to note in Fig. 11 that the apparent activation energy of the CO–NO reaction over Rh/Al_2O_3 changes with the gas-phase reactant composition. For the case of $P_{CO} = P_{NO} = 5 \times 10^{-3}$ atm (closed circles), the observed activation energy of ~47 kcal/mol can be rationalized based on a reaction mechanism where the dissociation of chemisorbed NO is the rate-limiting step and both CO and NO are in adsorption equilibrium (*37*). However, a tenfold reduction in the NO partial pressure ($P_{CO} = 5 \times 10^{-3}$ atm and $P_{NO} = 5 \times 10^{-4}$ atm; see closed squares) yielded a considerably lower apparent activation energy (~25 kcal/mol), indicating that the same mechanism does not apply. It is possible that at low P_{NO}, the assumption of NO adsorption equilibrium is not justified because of its limited adsorption rate. Further work is required to clarify the detailed reaction mechanism for this case.

V. CONCLUDING REMARKS

This paper describes the results of a comparative kinetic study of the $CO–O_2$ and CO–NO reactions over single crystal and supported Rh catalysts at realistic reactant pressures. For the $CO–O_2$ reaction, there is excellent agreement between both the specific rates and activation energies measured for the single crystal Rh(111) and alumina-supported Rh catalysts. The CO–NO reaction, on the other hand, exhibits substantially different activation energies and specific reaction rates over the two types of Rh catalysts. This indicates that the kinetics of CO–NO reaction, unlike the $CO–O_2$ reaction kinetics, are sensitive to changes in catalyst surface characteristics.

The kinetic data for $CO–O_2$ and CO–NO reactions over Rh(111) and Rh/Al_2O_3 were analyzed using mathematical models which account for the individual elementary reaction steps established from ultrahigh vacuum studies of the interactions of CO, NO, and O_2 with bulk Rh surfaces. The model, when used with the parameter values similar to those reported in the surface science literature, can quantitatively fit the CO oxidation rate data over both the single crystal and supported Rh catalysts. The rate data for the CO–NO reaction over Rh(111) can

also be well described by the surface chemistry reaction model. However, model calculations for the CO–NO reaction over the Rh/Al_2O_3 catalyst suggest that the structure sensitivity observed for the CO–NO reaction may be related to a large difference in the NO dissociation rate between supported and unsupported Rh.

Such comparative kinetic studies are essential for establishing the correlation between single crystal and supported catalyst systems. Good correlation between these two catalyst systems (as is observed for the $CO-O_2$ reaction) would allow one to utilize the wealth of chemical information obtained from model surface studies to gain a detailed understanding of high surface area, supported metal catalysts. For the case of structure-sensitive reactions (such as the CO–NO reaction), a comparative kinetic study coupled with mathematical modeling approach can help identify the kinds of studies necessary to clarify the origins of the structure sensitivity between different catalyst systems and also provide useful insights for the development of improved catalysts.

VI. APPENDIX: NOMENCLATURE

- A preexponential factor (s^{-1})
- C reactant concentration in gas phase (mol/cm^3)
- E activation energy (kcal/mol)
- k rate constant, $A \exp[-E/R_gT]$ (s^{-1})
- M molecular weight (g/mol)
- P partial pressure of reactant (atm)
- R_g gas constant
- $\bar{R}$ rate of overall reaction (s^{-1})
- r rate for elementary reaction step (s^{-1})
- S initial sticking coefficient (dimensionless)
- T temperature (K)
- α parameter describing variation in activation energy with surface coverage (kcal/mol)
- θ surface coverage (dimensionless)
- σ area occupied by 1 mol of surface metal atoms (cm^2/mol)

ACKNOWLEDGMENT

One of the authors (D.W.G.) would like to acknowledge the partial support of this work by the Department of Energy, Office of Basic Energy Sciences, Division of Chemical Sciences.

REFERENCES

1. Blakely, D. W., Kozak, E., Sexton, B. A., and Somorjai, G. A., *J. Vac. Sci. Technol.* **13,** 1091 (1976).
2. Goodman, D. W., Kelley, R. D., Madey, T. E., and Yates, J. T., Jr., *in* "Proceedings, Symposium on Advances in Fischer-Tropsch Chemistry," 175th National Meeting of the American Chemical Society, Anaheim, Calif., March 1978.
3. Goodman, D. W., Kelley, R. D., Madey, T. E., and Yates, J. T., Jr., *J. Catal.* **63,** 226 (1980).
4. Goodman, D. W., *J. Vac. Sci. Technol.* **20,** 522 (1982).
5. Somorjai, G. A., *Surf. Sci.* **89,** 496 (1979).
6. Goodman, D. W., *Surf. Sci.* **123,** L679 (1982).
7. Fisher, G. B., Goodman, D. W., and Oh, S. H., in preparation.
8. Yao, H. C., and Rothschild, W. G., *J. Chem. Phys.* **68,** 4774 (1978).
9. Cavanagh, R. R., and Yates, J. T., Jr., *J. Chem. Phys.* **74,** 4150 (1981).
10. Berty, J. M., *Chem. Eng. Prog.* **70,** 78 (1974).
11. Engel, T., and Ertl, G., "Advances in Catalysis," Vol. 28, p. 1. Academic Press, New York, 1979.
12. Fisher, G. B., and Schmieg, S. J., *J. Vac. Sci. Technol.* **A1,** 1064 (1983).
13. Root, T. W., Schmidt, L. D., and Fisher, G. B., *Surf. Sci.* **134,** 30 (1983).
14. Matsushima, T., *J. Catal.* **85,** 98 (1984).
15. Thiel, P. A., Yates, J. T., Jr., and Weinberg, W. H., *Surf. Sci.* **82,** 22 (1979).
16. Castner, D. G., and Somorjai, G. A., *Surf. Sci.* **6,** 29 (1980).
17. Kellogg, G. L., *J. Catal.* **92,** 167 (1985).
18. Oh, S. H., and Carpenter, J. E., *J. Catal.* **80,** 472 (1983).
19. Wang, T., and Schmidt, L. D., *J. Catal.* **71,** 411 (1981).
20. Zhu, Y., and Schmidt, L. D., *Surf. Sci.* **129,** 107 (1983).
21. Somorjai, G. A., "Principles of Surface Chemistry," Prentice–Hall, Englewood Cliffs, N.J., 1972.
22. Herz, R. K., and Marin, S. P., *J. Catal.* **65,** 281 (1980).
23. Yates, J. T., Jr., Thiel, P. A., and Weinberg, W. H., *Surf. Sci.* **82,** 45 (1979).
24. Engel, T., *J. Chem. Phys.* **69,** 373 (1978).
25. Monroe, D. R., and Merrill, R. P., *J. Catal.* **65,** 461 (1980).

26. Weinberg, W. H., Comrie, C. M., and Lambert, R. M., *J. Catal.* **41,** 489 (1976).
27. McCabe, R. W., and Schmidt, L. D., *Surf. Sci.* **66,** 101 (1977).
28. Falconer, J. L., and Madix, R. J., *J. Catal.* **48,** 262 (1977).
29. Taylor, J. L., and Weinberg, W. H., *Surf. Sci.* **78,** 259 (1978).
30. Madix, R. J., and Benziger, J., *Ann. Rev. Phys. Chem.* **29,** 285 (1978).
31. Chan, C.-M., Aris, R., and Weinberg, W. H., *Appl. Surf. Sci.* **1,** 360 (1978).
32. Thiel, P. A., Williams, E. D., Yates, J. T., Jr., and Weinberg, W. H., *Surf. Sci.* **84,** 54 (1979).
33. Campbell, C. T., and White, J. M., *Appl. Surf. Sci.* **1,** 347 (1978).
34. Baird, R. J., Ku, R. C., and Wynblatt, P., *Surf. Sci.* **97,** 346 (1980).
35. Arai, H., and Tominaga, H., *J. Catal.* **43,** 131 (1976).
36. Solymosi, F., and Sarkany, J., *Appl. Surf. Sci.* **3,** 68 (1979).
37. Hecker, W. C., and Bell, A. T., *J. Catal.* **84,** 200 (1983).
38. Chin, A. A., and Bell, A. T., *J. Phys. Chem.* **87,** 3700 (1983).
39. Hecker, W. C., and Bell, A. T., *J. Catal.* **85,** 389 (1984).
40. Root, T. W., Schmidt, L. D., and Fisher, G. B., *Surf. Sci.* **150,** 173 (1985).
41. Root, T. W., Fisher, G. B., and Schmidt, L. D., submitted for publication.
42. McCarthy, E., Zahradnik, J., Kuczynski, G. C., and Carberry, J. J., *J. Catal.* **39,** 29 (1975).
43. Cant, N. W., *J. Catal.* **62,** 173 (1980).
44. Ladas, S., Poppa, H., and Boudart, M., *Surf. Sci.* **102,** 151 (1981).
45. Campbell, C. T., Shi, S.-K., and White, J. M., *Appl. Surf. Sci.* **2,** 382 (1979).
46. Campbell, C. T., and White, J. M., *J. Catal.* **54,** 289 (1978).
47. Fisher, G. B., and DiMaggio, C. L., unpublished results.
48. Baetzold, R. C., and Somorjai, G. A., *J. Catal.* **45,** 94 (1976).
49. Levenspiel, O., "Chemical Reaction Engineering," 2nd Ed., p. 32. Wiley, New York, 1972.
50. Miyazaki, E., and Yasumori, I., *Surf. Sci.* **57,** 755 (1976).
51. Yao, H. C., Yao, Y.-F., Yu, and Otto, K., *J. Catal.* **56,** 21 (1979).
52. van't Blik, H. F. J., van Zon, J. B. A. D., Huizinga, T., Vis, J. C., Koningsberger, D. C., and Prins, R., *J. Amer. Chem. Soc.* **107,** 3139 (1985).